Acta Crystallographica Section D
Biological Crystallography
ISSN 0907-4449

3D EXAFS refinement of the Cu site of azurin sheds light on the nature of structural change at the metal centre in an oxidation–reduction process: an integrated approach combining EXAFS and crystallography

Kan-Cheung Cheung,[a,b] Richard W. Strange[b] and S. Samar Hasnain[a,b]*

[a]Faculty of Applied Sciences, De Montfort University, Leicester LE1 9BH, England, and [b]CCLRC Daresbury Laboratory, Warrington, Cheshire WA4 4AD, England

Correspondence e-mail: s.hasnain@dl.ac.uk

Received 3 September 1999
Accepted 1 March 2000

Three-dimensional information is obtained for the Cu site in azurin at very high resolution by combining high-resolution crystallographic structures and EXAFS data for the oxidized and reduced form of the protein. This combined approach has allowed us to define the subtle structural changes (<0.1 Å) which take place at the Cu site during a single-electron redox process.

1. Introduction

Metalloproteins utilize the chemistry of metals to their advantage to perform varied biological functions with specificity and control. These chemical reactions are often accompanied by only small structural changes around the metal atom and structures approaching atomic resolution are often required to understand them. It is perhaps fair to claim that nowhere in the determination of molecular structures are precision and accuracy more at a premium than in the case of metalloproteins. It is thus understandable why high-resolution (<2 Å) structure determination of metalloproteins has attracted so much attention (see, for example, Dauter *et al.*, 1997). Unfortunately, it is often impossible to obtain atomic resolution (<1.2 Å) crystallographic data owing to various factors including inherent diffraction limits of the protein crystals arising from static disorder. Thus, as of 1 April 1999 (Hasnain & Hodgson, 1999), there are a total of 165 structures known for copper proteins but only amicyanin ($M_W \simeq$ 11.5 kDa) and plastocyanin ($M_W \simeq$ 10.5 kDa), both cupredoxins, have been determined to a resolution approaching atomic resolution, namely 1.31 Å (Cunane *et al.*, 1996) and 1.33 Å (Guss *et al.*, 1992), respectively. In such cases, EXAFS can be used to provide very high (atomic or better) resolution information about the metal centre.

Important developments of the EXAFS technique have taken place in recent years, such as curved or spherical wave multiple-scattering theory, physically more accurate electronic potentials and phase shifts and the incorporation of interatomic distance constraints and restraints (Binsted *et al.*, 1992; Ellis & Freeman, 1995; Gurman *et al.*, 1984, 1986; Mustre de Leon *et al.*, 1991; Natoli *et al.*, 1986; Rehr *et al.*, 1991). Advances in X-ray fluorescence detector technology (Cramer *et al.*, 1988; Derbyshire *et al.*, 1999) have enabled good-quality EXAFS data to be obtained from relatively low protein concentrations (<1 m*M*) and further improvements are anticipated with the next generation of synchrotron sources, including measurements of kinetic processes. However, the complete three-dimensional structural information necessary

to understand the chemistry of a metal site in a protein has so far been lacking in the EXAFS approach. Thus, despite the high resolution of the EXAFS technique and its equal applicability to crystalline and aqueous states, its full power has not been achieved. In this paper, the results of a new refinement approach for EXAFS data are reported for azurin II from *Alcaligenes xylosoxidans*, where coordinates from our 1.75 Å crystallographic structures (Dodd *et al.*, 2000) are used as the starting model. The aim of this study is to demonstrate that the combination of high-resolution crystallographic information and ultrahigh-resolution EXAFS may provide a powerful approach for studying the structure–function relationships in proteins, particularly when subtle structural changes are associated with a chemical reaction. This approach is also likely to be of interest where crystallographic information is available for some state of a protein but not others; for example, the resting-state structure may be known but crystallographic data on reactive intermediates may be lacking. In such circumstances, EXAFS data on different states of the protein may be solved by the combined approach to predict structural features of these intermediates. Since EXAFS is a relatively short-range phenomenon, the information derived from it is limited to a specific volume ($\sim$550 Å^3) of the protein centred on the metal atom.

2. Method

2.1. 3D EXAFS analysis

The crystal structure coordinates of oxidized and reduced azurin II, in standard Brookhaven Protein Data Bank (PDB) format (Bernstein *et al.*, 1977), were read into the Daresbury Laboratory EXAFS analysis program *EXCURV*98. The Cu atom was placed at the origin of the coordinate system. For both oxidized and reduced structures, a total of 21 atoms (see Fig. 3) belonging to the five metal ligands lie within 4.5 Å of the Cu atom. The three-dimensional arrangement of the copper ligands as found in the two crystal structures is preserved using this method.

In the 'conventional' method of EXAFS analysis, this three-dimensional information would be absent because of averaging, *e.g.* the relative positions of the two histidine ligands about the metal would be lost because they would be treated as one unit with coordination number of two (*e.g.* Blackburn *et al.*, 1987, 1991; Murphy *et al.*, 1997; Strange *et al.*, 1987; Strange, Reinhammar *et al.*, 1995). Similarly, the positions of the remaining ligands would not be maintained. Thus, the 'conventional' method is restricted to providing distance information only together with some limited intra-ligand geometrical data using restraints.

The approach conducted here is made viable by direct inclusion of the geometrical information derived from a metalloprotein crystal structure and by incorporating inter-ligand multiple-scattering pathways in the theoretical calculation of the EXAFS. In principle, these calculations allow determination of the entire X-ray absorption spectrum, including the near-edge region (Binsted & Hasnain, 1996). The main disadvantage of the new approach is that averaging can no longer be applied to minimize the number of parameters used to fit the EXAFS. To avoid problems of underdetermination of the data, rigid-body (constrained) fitting was first used. The data were then refined against a set of 'idealized' interatomic bond lengths taken from the well established Engh and Huber library of crystallographic distance restraints (Engh & Huber, 1991). We have previously applied these methods, adopted from the constrained–restrained refinement procedures in small-molecule and protein crystallography (Konnert & Hendrickson, 1980), to the EXAFS of the type-1 and type-2 copper sites of the nitrite reductase from *A. xylosoxidans* (Strange, Dodd *et al.*, 1995) and to the type-2 copper site of oxidized and reduced bovine CuZn superoxide dismutase (Murphy *et al.*, 1997). This is the first application to

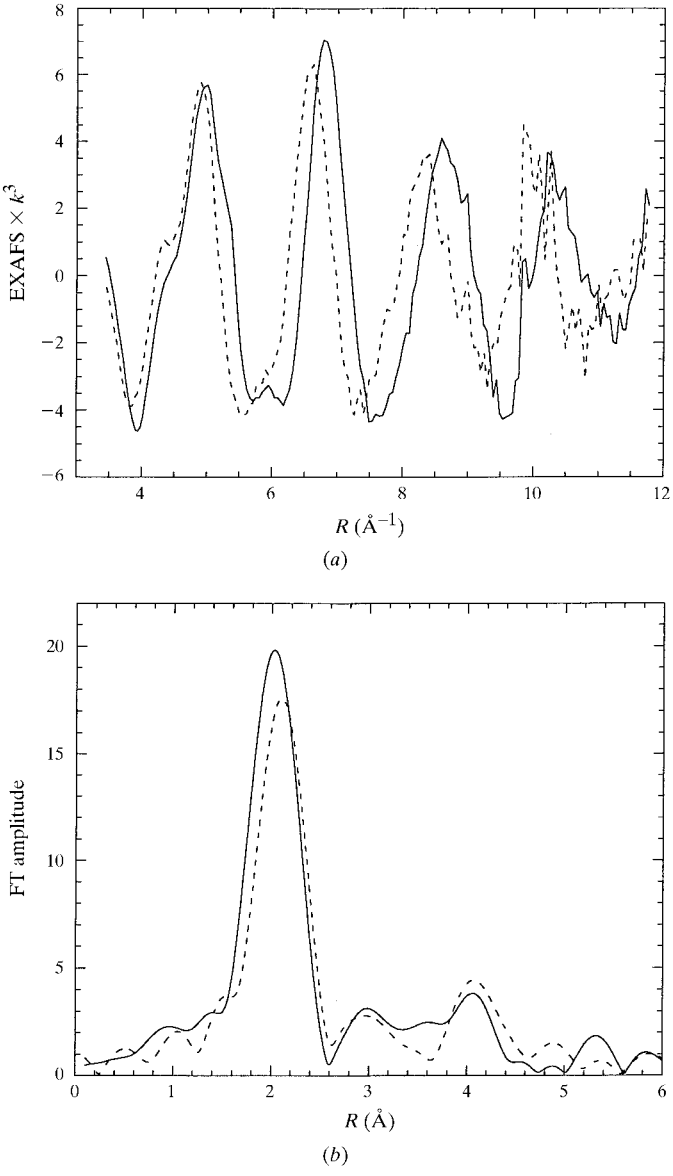

Figure 1
(*a*) k^3-weighted Cu K edge EXAFS spectra and (*b*) corresponding Fourier transforms for oxidized (solid line) and reduced (dashed line) azurin II.

a full three-dimensional analysis of EXAFS data which directly employs crystallographic information. It was accomplished in three stages, beginning with the fit to the EXAFS given by the original crystal structure coordinates of the oxidized and reduced protein. This was then followed by constrained and restrained refinement of the data as described below. For completeness, alternative initial parameter sets were used to test the uniqueness of the fits. The EXAFS fit parameters for the oxidized state were used as the starting parameters for the reduced data and *vice versa*. Very similar fit index and fit parameters (within 0.01 Å for the four closest ligating atoms) were obtained in both cases for each EXAFS spectrum.

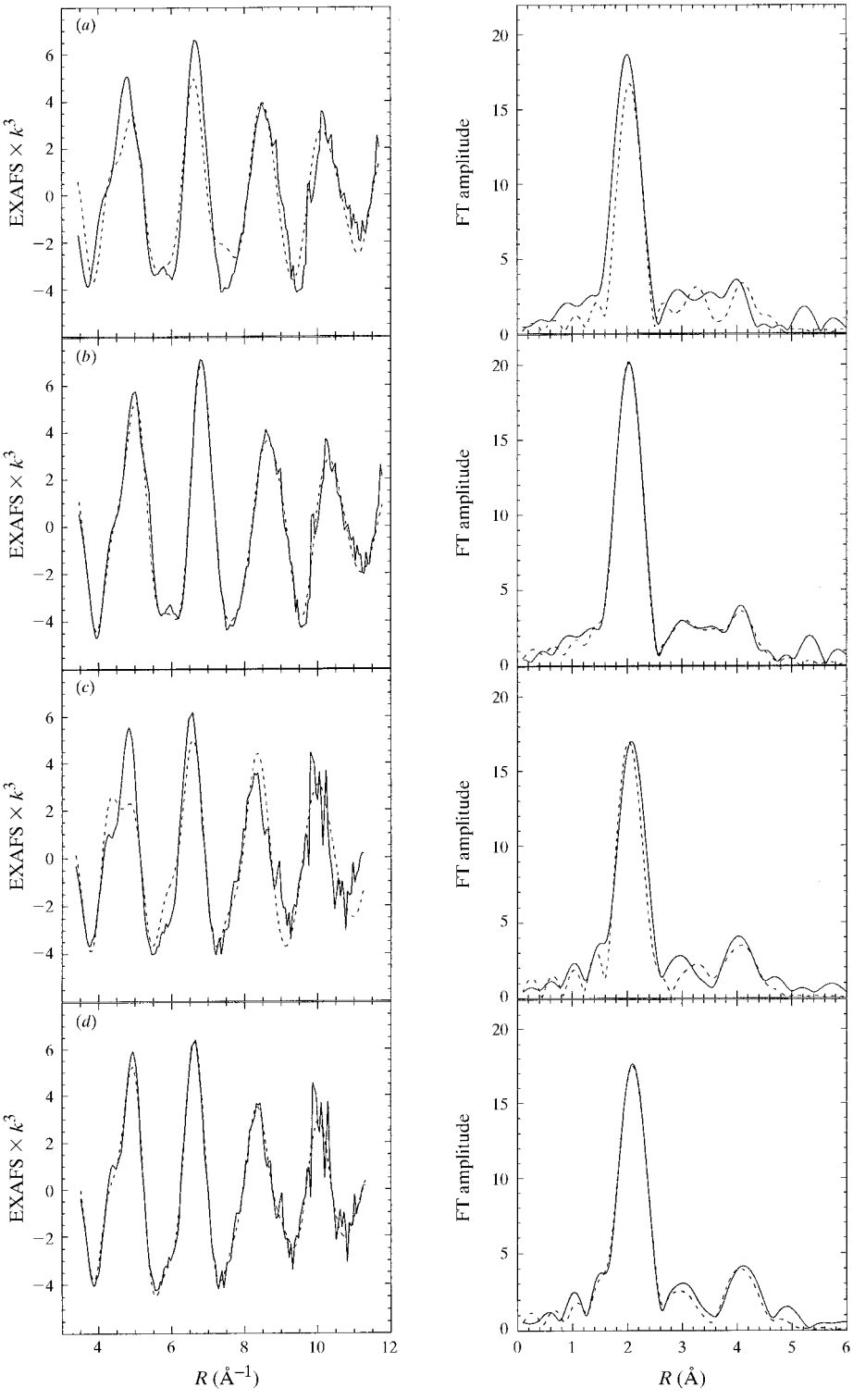

Figure 2
Simulations (dashed lines) of the k^3-weighted Cu K edge EXAFS spectra of azurin II with their corresponding Fourier transforms for the oxidized protein with (*a*) crystal structure coordinates, (*b*) after refinement, and for the reduced protein with (*c*) crystal structure coordinates, (*d*) after refinement.

2.1.1. EXAFS fits using crystallographic coordinates. Simulations of the oxidized and reduced azurin II EXAFS data were first carried out using the relevant crystal structure coordinates, refining only the Fermi energy (*i.e.* absorption threshold energy, E_f) to give the best match between the experimental and theoretical spectra. The Debye–Waller terms of the nearest neighbour atoms were adjusted manually to give an acceptable amplitude match on the first Fourier transform peak. Refining these terms tended to give a physically unrealistic result, already an indication that changes to the crystallographic parameters are required to fit the EXAFS. The values used were 0.004, 0.004 and 0.002 Å^2, respectively, for the two N(His) atoms and the S(Cys) atom. The remaining atoms were assigned Debye–Waller terms of 0.010 Å^2.

2.1.2. Constrained three-dimensional EXAFS refinements of azurin II. Rigid-body refinement was carried out starting with the oxidized and reduced crystal structure coordinates. The k range was 9.1 Å^{-1} for the oxidized protein and 8.6 Å^{-1} for the reduced protein. The bandwidth of the radial distances was 3.0 Å in both cases. The number of independent data points in each EXAFS spectrum was therefore 19.4 and 18.4, respectively (Binsted *et al.*, 1992; Stern *et al.*, 1992). Constrained refinement required 12 parameters: the two histidine Cu—N(His) distances, the S(Cys) distance, the O(Gly) distance, the S(Met) distance, the Debye–Waller terms for these atoms [with the two N(His) atoms constrained to the same value

during refinement] and E_f. In addition, each histidine ligand was rotated about the normal to the Cu—N(His) vector.

2.1.3. Restrained 3D EXAFS refinements of azurin II. The total of 21 atoms within 4.5 Å of the Cu atom means that 21 distances need to be included. The Debye–Waller terms for atoms at similar distances for a given ligand type were grouped together to give a further 14 possible refinable parameters for the 21 atoms. In addition to this total, the polar angles for each atomic coordinate (θ and φ) also have to be considered. If all 21 θ and 21 φ angles for the atoms were included in the refinement, it would result in nearly 80 parameters including E_f. The problem becomes significantly underdetermined in this case and therefore some sensible adjustments to the parameter list must be made to avoid this outcome. Firstly, it was decided to eliminate all θ angles from the analysis, keeping them at their crystallographic values. This decision is sensible as it also ensures that the imidazole rings will retain their planar configuration during the analysis. Secondly, of the 21 φ angles, only the eight φ angles belonging to the second- and third-shell atoms of the two imidazole rings were selected for refinement. This is justified because only these atoms provide significant intraligand multiple-scattering contributions to the EXAFS. Thus, the 42 angular terms are reduced to only eight. Thirdly, in addition to the Debye–Waller terms for the five atoms directly coordinated to the copper, only the Debye–Waller terms for the second- and third-shell atoms of the imidazole ring of the histidine ligands were selected for refinement, reducing the number of refinable terms from 14 to six. The remaining Debye–Waller terms were fixed at a value of 0.010 Å^2. The total number of parameters considered for refinement was therefore 36 including E_f. In calculating the number of additional observations allowed for restrained refinement, two-dimensional restraints on the bond distances were applied (Binsted *et al.*, 1992). This gave 27 additional observations. The maximum numbers of refinable parameters permitted were 46 and 45, so that the ratios of observations to parameters were 1.27 and 1.25, respectively, for the oxidized and reduced data.

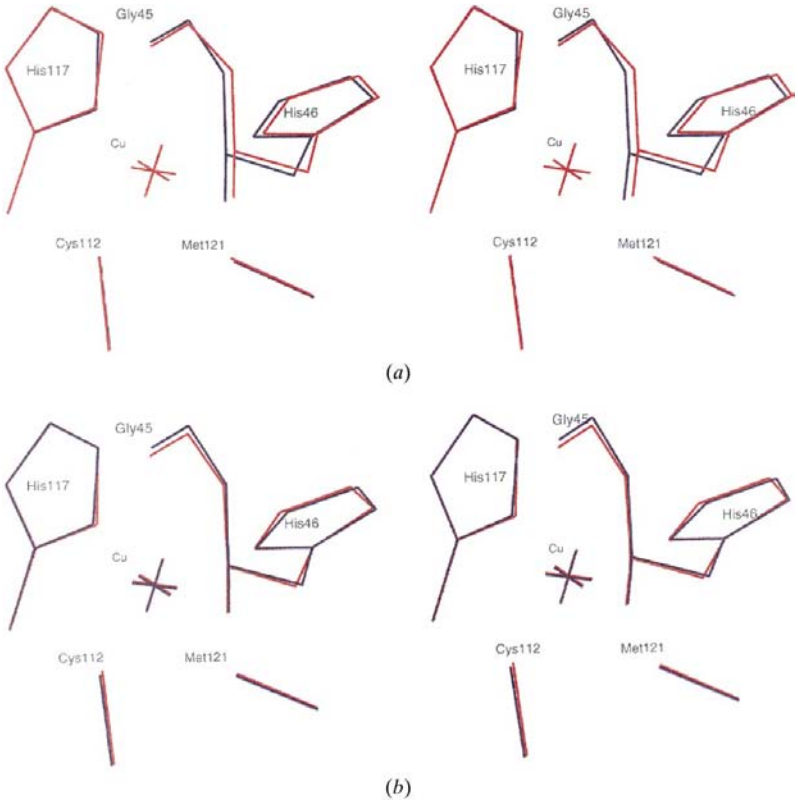

Figure 3
(*a*) Crystallographic (red) and EXAFS (blue) derived stereochemistry of *A. xylosoxidans* azurin II for the oxidized site. (*b*) Stereochemistry of the oxidized (red) and reduced (blue) copper sites determined by EXAFS refinements of the crystal structure data.

2.2. Sample preparation

Azurin II was extracted and purified from *A. xylosoxidans* as described previously (Dodd *et al.*, 1995). All protein manipulations were performed at 277 K and all chemicals were reagent grade and were used without further purification. Water was deionized using a Elgastat water treatment system. Approximately half of the protein solution was removed to prepare the reduced protein. The remaining oxidized sample was concentrated to a volume of ∼400 µl. Reduction of the protein was performed by purging the sample in an Amicon stirred concentration cell pressurized with ultrapure argon, in approximately 2 ml of appropriate buffer. The volume was reduced to 400 µl and then a small aliquot (10 µl) of 1 *M* sodium ascorbate dissolved in degassed buffer was added. Bleaching of the intense blue colour of the samples was taken as a visual indication of reduction. Final stage protein concentrations, to ∼3 m*M* in copper content, were performed using Centricon-10 concentrators from Amicon Ltd. Phosphate buffer (0.1 *M*) at pH 6.0 was used for the EXAFS experiments. The samples were frozen in liquid nitrogen prior to use. The integrity of the samples before and after exposure to X-rays was checked by X-band EPR measurements at 77 K on a Jeol JES-RE2X spectrometer.

2.3. Data collection and processing

X-ray absorption spectra at the Cu *K* edge were measured in fluorescence mode with a 13-element Ge solid-state detector on wiggler EXAFS station 9.2 at the Synchrotron Radiation Source, Daresbury Laboratory. The station was equipped with an Si(220) order-sorting double-crystal monochromator which was set up to perform harmonic rejection at 50%. The electron-beam energy was 2 GeV, with an average current of 170 mA. The X-ray energy was calibrated by scanning a 5 µm copper foil in transmission mode and setting the first inflection point on the absorption edge equal

to 8982 eV. Calibration of the Ge detector was achieved by measuring the X-ray fluorescence of a 15 m*M* copper nitrate atomic absorption standard solution at room temperature. Measurements were carried out using QuEXAFS mode (Frahm, 1989; Murphy *et al.*, 1995) at approximately 80 K using a liquid-nitrogen cryostat. Data were collected in k space using a k^3-weighted regime for the counting time, with a maximum scan time of 600 s. A total of 18 scans each were recorded on oxidized and reduced azurin II. X-ray damage and changes in the oxidation state of the protein were monitored by comparison of successive EXAFS data sets during data collection; no changes were observed. The scans were averaged after checking the output of each detector element individually for glitches or anomalies in the data. After calibration of the monochromator angle to energy, the EXAFS was normalized to a unit Cu atom and extracted from the background absorption using the Daresbury Laboratory program *EXBACK* (Morrell *et al.*, 1989). The EXAFS data were converted into k space using $k = [2m_e(E - E_f)/\hbar^2]$, where E is the energy of the incident X-ray radiation and k is the photoelectron wavevector. Analysis of the EXAFS data was performed using the non-linear least-squares program *EXCURV*98, which calculates the theoretical EXAFS function using fast curved-wave theory (Gurman *et al.*, 1984, 1986) and incorporates multiple scattering up to fifth order. This version of the program includes interligand scattering terms in the calculations (Binsted & Hasnain, 1996). The phase shifts employed were calculated using Hedin–Lundqvist exchange and correlation potentials (Hedin & Lundqvist, 1969; Rehr *et al.*, 1991) and were first tested (Cheung, 1998) by fitting the Cu K edge EXAFS of two model compounds, copper tetrakis(imidazole) dinitrate (McFadden *et al.*, 1975) and copper disulfide (King & Prewitt, 1979).

3. Results and discussion

In the denitrifying bacterium *A. xylosoxidans*, the reduction of nitrite to nitric oxide is accomplished by a copper-containing nitrite reductase (Abraham *et al.*, 1993). The bacteria synthesizes two biochemically distinct azurins, each of which is equally capable of donating electrons to the nitrite reductase (Dodd *et al.*, 1995); this electron donation *via* complex formation is an essential step for the enzyme turnover. It remains unknown how the complex dissociates once the electron is transferred and whether this dissociation is triggered by structural changes in the donor protein. Crystallographic studies of a number of cupredoxins including azurins have suggested that little or no change takes place upon oxidation/reduction (*e.g.* Dodd *et al.*, 2000); the exceptions being amicyanin (Durley *et al.*, 1993) and plastocyanin (Guss *et al.*, 1986), where at low pH one of the copper-ligating histidine is moved by nearly 1 Å. In contrast, EXAFS data have suggested a significant change for azurins (Groenveld *et al.*, 1986), while confirming the dissociation of one of the His ligands in amicyanin (Lommen *et al.*, 1991) and plastocyanin (Penner-Hahn *et al.*, 1989; Murphy *et al.*, 1991).

Table 1
Statistics for different EXAFS fit models to oxidized and reduced azurin II.

	Oxidized EXAFS	Reduced EXAFS
k range (Å^{-1})	9.1	8.6
Radial bandwidth (Å)	3.0	3.0
Crystal structure fit		
Number of observations	19	18
Number of parameters	1	1
Fit index	3.46	3.90
R factor (%)	37.8	38.2
Constrained fit		
Number of observations	19	18
Number of parameters	12	12
Fit index	0.93	1.66
R factor (%)	19.2	23.8
Restrained fit		
Additional observations	27	27
Number of observations	46	45
Number of parameters	36	36
Fit index	0.49	0.85
R factor (%)	13.6	16.8
Deviation from Engh and Huber (%)	0.88	0.93

3.1. Summary of crystallographic information

We have previously published the crystallographic structure of oxidized azurin II at 1.9 Å resolution (Dodd *et al.*, 1995). Subsequently, the structures of oxidized and reduced azurin II have been refined to 1.75 Å resolution using identical protocols (Dodd *et al.*, 2000). There are three strong ligands arranged in a distorted trigonal plane around the Cu atom, namely His46 N^{δ}, His117 N^{δ} and Cys112 S^{γ}. In addition, two groups are found axial to the copper, one being Met121 S^{δ} and the other the carbonyl O atom of Gly45. The two Cu sites show little detectable difference in the metal environment when the oxidation state of the copper is altered. The largest changes in the Cu–ligand distances are increases of 0.03 Å in the Cu—Gly45 and Cu—His117 bonds and 0.02 Å in the Cu—Cys112 bond on going from the oxidized to the reduced state. Additionally, the orientations (θ and φ angles) of the Cu ligands are identical to within 1° in the two forms. These differences between the two structures are within the experimental errors of the crystallographic determination. Similar results were found for the crystallographic structures at 1.8 Å resolution for the oxidized and reduced azurin from *A. denitrificans* (Shepard *et al.*, 1990).

3.2. EXAFS of oxidized and reduced azurin II

3.2.1. Qualitative analysis. The X-ray absorption measurements tell a different story about the immediate environment of copper in the reduced *versus* native oxidized state. The k^3-weighted normalized EXAFS spectra, shown in Fig. 1, have the same general features, owing to the fact that the two forms of the protein have the same set of ligands around the copper. The Fourier transforms for both spectra have the 'signature' triple-peak profile characteristic of imidazole coordination. The major peak in the transform arises from backscattering from the inner-shell histidine N

Table 2
EXAFS fit parameters using Engh and Huber restraints compared with crystallographic coordinates for oxidized and reduced *A. xylosoxidans* azurin II.

$2\sigma^2$ is the Debye–Waller term for each atom.

	Oxidized protein			Reduced protein		
	Crystallographic	EXAFS		Crystallographic	EXAFS	
Ligand	distance (Å)	Distance (Å)	$2\sigma^2$ (Å^2)	distance (Å)	Distance (Å)	$2\sigma^2$ (Å^2)
His117	1.99	1.94 (0.02)	0.002	2.02	2.01 (0.02)	0.002
His46	2.04	1.86 (0.02)	0.002	2.03	1.91 (0.02)	0.002
Cys112	2.14	2.12 (0.02)	0.001	2.16	2.19 (0.02)	0.001
Gly45	2.72	2.82 (0.05)	0.012	2.75	2.98 (0.05)	0.021
Met121	3.26	3.39	0.055	3.26	3.35	0.058
E_f (eV)	−9.27	0.61		−2.82	0.09	

atoms and the S atom from cysteine. The two outer-shell peaks arise mainly from strong multiple-scattering contributions from the five-atom imidazole rings of His46 and His117. However, the EXAFS spectra are significantly different in detail. The EXAFS frequency has become higher in going from the oxidized to the reduced state. This corresponds to longer (overall) atomic distances (or scattering paths) and implies that one or more of the ligands have moved away from the copper. Some additional structural changes must also have taken place in the outer-shell atoms to give differences in the k region between 4.0 and 6.0 Å^{-1}, where multiple scattering makes a significant contribution to the EXAFS spectra. A closer look at the difference between the two transforms reveals that the whole of the triple-peak signature is shifted to longer distances in the reduced case. This also suggests that at least one of the two histidines has moved away from the copper upon reduction. The EXAFS data thus reveals significant qualitative structural differences at the copper site between the oxidized and reduced states of the protein. Such changes may also occur in the crystalline state, but the lack of any significant differences (*i.e.* larger than the experimental errors) in the crystal structures suggests that the current resolution of 1.75 Å is not sufficient for a detailed examination of the chemistry of the redox centre.

3.2.2. Simulation of EXAFS data and quantitative analysis. The simulation of the EXAFS of the oxidized protein using the crystallographic coordinates is shown in Fig. 2(*a*) (left-hand panel) and yields a fit index[1] of 3.46 and an R factor of 37.8%. The theoretical EXAFS has approximately the correct phase and amplitude at high k, but the phase and amplitude match is poor at lower k (<6 Å^{-1}). The first peak of the theoretical Fourier transform (Fig. 2*a*, right-hand panel) is narrower than the experimental peak and its maximum occurs at a longer distance. The position of this peak is correlated with the positions of the second and third peaks in the theoretical transform, as though the entire fingerprint triple-peak transform has been shifted to longer distances. This observation strongly suggests that at least one of the two crystallographic histidine distances is too long to fit the EXAFS spectrum. The simulation of the EXAFS of the reduced protein using crystallographic coordinates is shown in Fig. 2(*c*), giving a fit index of 3.90 and an R factor of 38.2%. To a first approximation, there is again a reasonable phase match between the theory and experiment above 6 Å^{-1}, but the amplitude match is poor. The major peak of the theoretical Fourier transform has its maximum at a shorter distance than the experimental transform curve; the position of the second theoretical transform peak is incorrect, while the third peak corresponds reasonably well with the experimental curve. The crystallographic oxidized and reduced structures provide a reasonable overall initial fit to both the data sets. Nevertheless, significant modifications to the structures are needed to give an adequate account of the EXAFS data set in detail.

Rigid-body refinement of the oxidized data resulted in a threefold decrease in the fit index (0.93) and a twofold decrease in the R factor (19.2%). For the reduced EXAFS, the improvement was a decrease in fit index from 3.90 to 1.66 and in R factor from 38.2 to 23.8%. At this stage of the refinement, the main advance was in fitting the contribution to the experimental EXAFS from the nearest-neighbour (bonding) atoms. A subsequent cycle of restrained refinement for both data sets produced additional improvements to the simulations, decreasing the fit index for each case by about half. The improvements in this cycle of refinement were chiefly a consequence of changes in the positions of the 'outer-shell' atoms of the Cu ligands. The deviation from the Engh and Huber distance restraints was 0.9% for both data sets. The different refinements are summarized in Table 1. The final fits to the EXAFS data are shown in Figs. 2(*b*) (oxidized) and 2(*d*) (reduced) and the Cu–ligand EXAFS distances are compared with the crystal structure values in Table 2.

3.2.3. Comparison of three-dimensional EXAFS and crystallographic data. The stereochemistry of the oxidized copper site determined by the EXAFS refinement is compared with its crystallographic counterpart in Fig. 3(*a*). Both of the histidine ligands refined to shorter distances than their crystal structure values by 0.05 Å for His117 and 0.18 Å for His46. The low Debye–Waller terms for the N(His) and S(Cys) atoms signifies strong interactions with the Cu atom. By contrast, the S(Met) atom has a much larger Debye–Waller term (0.055 Å^2), suggesting a very weak bonding interaction with the Cu atom, and the EXAFS-derived distance is longer (3.39 Å) than in the crystal structure (3.26 Å). The difficulty of detecting the weak methionine–copper interaction has been noted before in EXAFS studies of type-1 copper proteins (for examples, see Penner-Hahn *et al.*, 1989; Scott *et al.*, 1982). The shortening of copper–histidine distances in the EXAFS of

[1] The fit index is defined as $\Phi = \sum_i (1/\sigma_i^2)\{k^3[\chi^{\rm exp}(k_i) - \chi^{\rm the}(k_i)]\}^2$, where $\sigma = \sum_j k^3|\chi^{\rm exp}(k_j)|$ and $\chi^{\rm exp}$ and $\chi^{\rm the}$ are the experimental and theoretical EXAFS, respectively. The R factor is defined as $R = 100 \times \sum_i (1/\sigma_i)k^3|\chi^{\rm exp}(k_i) - \chi^{\rm the}(k_i)|$.

Table 3
Summary of the crystallographic (PX) and EXAFS derived geometrical information for the Cu sites in oxidized and reduced azurin II.

	Oxidized PX	Reduced PX	Oxidized EXAFS	Reduced EXAFS
Ligand distances (Å)				
Cu—O(45)	2.72	2.75	2.82	2.98
Cu—$N^{\delta1}$(46)	2.04	2.03	1.86	1.91
Cu—S^{γ}(112)	2.14	2.16	2.12	2.19
Cu—$N^{\delta1}$(117)	1.99	2.02	1.94	2.01
Cu—S^{δ}(121)	3.26	3.26	3.39	3.35
Angle at Cu atom (°)				
O(45)—Cu—$N^{\delta1}$(46)	77.8	76.2	77.8	76.2
O(45)—Cu—S^{γ}(112)	104.1	105.1	104.1	105.1
O(45)—Cu—$N^{\delta1}$(117)	86.4	86.2	86.5	86.3
O(45)—Cu—S^{δ}(121)	148.4	147.4	148.4	147.4
$N^{\delta1}$(46)—Cu—S^{γ}(112)	132.6	133.1	132.6	133.1
$N^{\delta1}$(46)—Cu—$N^{\delta1}$(117)	106.4	106.4	106.4	106.4
$N^{\delta1}$(46)—Cu—S^{δ}(121)	73.9	74.4	73.9	74.4
S^{γ}(112)—Cu—$N^{\delta1}$(117)	121.1	120.5	121.0	120.5
S^{γ}(112)—Cu—S^{δ}(121)	105.3	105.1	105.3	105.1
$N^{\delta1}$(117)—Cu—S^{δ}(121)	88.3	89.0	88.3	89.0
Angles at ligating atoms (°)				
45 C—O—Cu	135.6	135.5	134.9	135.1
46 C^{γ}—$N^{\delta1}$—Cu	129.1	129.7	132.7	130.2
46 $C^{\varepsilon1}$—$N^{\delta1}$—Cu	121.1	120.6	120.8	126.3
112 C^{β}—S^{γ}—Cu	113.3	112.8	113.2	120.7
117 C^{γ}—$N^{\delta1}$—Cu	126.8	126.9	128.1	129.3
117 $C^{\varepsilon1}$—$N^{\varepsilon1}$—Cu	123.4	123.5	124.2	124.7
121 C^{γ}—S^{δ}—Cu	141.6	145.4	nd†	nd
121 C^{ε}—S^{δ}—Cu	99.5	97.6	97.3	98.0
Cu—NNS plane‡	−0.01	−0.01	+0.01	+0.00

† nd – not determined. ‡ In the Cu—NNS plane distances, '+' refers to displacement towards Gly45 O.

type-1 copper proteins compared with their crystallographically determined values has also been remarked upon (*e.g.* Romero *et al.*, 1994). The Cu—O Gly45 is 0.1 Å longer than the crystallographic value and has a Debye–Waller term of 0.012 $Å^2$, indicating a much stronger interaction with the metal than the weak methionine interaction. These values for the Cu–ligand distances are consistent with previous analysis of type-1 proteins using averaged sets of radial parameters (Lommen *et al.*, 1991; Murphy *et al.*, 1991; Strange *et al.*, 1996; Strange, Reinhammar *et al.*, 1995), but the use in the present case of three-dimensional refinement has allowed us to define the whole of the stereochemistry of the oxidized azurin for the first time using EXAFS data.

For the reduced protein, the Cu—S(Cys) distance determined by EXAFS was 0.03 Å longer than the crystal structure value and one of the two histidine distances (Cu–His46) was shorter than in the crystal structure by 0.12 Å. The position of the S(Met) ligand was again weakly determined, with a Debye–Waller term of 0.058 $Å^2$ with a broad minimum centred on 3.35 Å. The Cu—O(Gly) distance increased to 2.98 Å.

3.2.4. Structural changes at the Cu site upon reduction. The copper coordination in the two EXAFS-derived structures are compared in Fig. 3(*b*) and shows a more significant change between the oxidized and reduced copper sites than is suggested by the 1.75 Å crystal structures. There is an increase in each of the Cu–ligand distances consistent with reduction of the Cu atom. The individual movements, which are what is measured by crystallography, are small, but the overall changes in bond distances owing to a number of concerted movements are significant and are what is measured by EXAFS. Thus, the increase in Cu—S(Cys) bond upon reduction is 0.07 Å as determined by EXAFS while it is 0.02 Å by crystallography. The Cu—N(His) bond lengths increase by 0.05–0.07 Å and the Cu—O(Gly) bond length by 0.16 Å. These changes are insignificant at the resolution of the crystal structure but are well beyond the error limits of the EXAFS determinations, which are ±0.02 Å for the Cu–histidine and Cu—S(Cys) distances and ±0.05 Å for the O(Gly) distance. The S(Met) ligand does not contribute significantly to the EXAFS for either oxidation state. Table 3 provides a complete summary of the three-dimensional information for the Cu site in the two redox states of azurin. A closer examination of this table suggests that the crystallographic distance of His46 deviates from the three-dimensional EXAFS value by twice as much as any other distance. In the oxidized form a difference of 0.18 Å is found, while for the reduced form a difference of 0.12 Å is obtained. The larger deviation of this ligand distance from EXAFS may represent a tighter stereochemical restraint on this residue in crystallographic refinement.

4. Conclusions

An integrated approach based on high-resolution crystallographic structure and EXAFS has allowed us to define structural changes which take place at the Cu site in azurin upon a single-electron redox process. The Cu–ligand distances change by 0.05–0.07 Å and can only be confidently defined crystallographically at atomic or better resolution. This example illustrates that in the absence of such resolutions, a combination of high-resolution crystallographic structure and 3D EXAFS refinement is a powerful approach. The method should be equally applicable to structures at medium or even lower resolution.

References

Abraham, Z. H. L., Lowe, D. J. & Smith, B. E. (1993). *Biochem. J.* **296**, 885.

Bernstein, F. C., Koetzle, T. F., Williams, G. J. B., Meyer, F. M. Jr, Brice, M. D., Rodgers, J. R., Kennard, O., Shimanouchi, T. & Tasumi, M. (1977). *J. Mol. Biol.* **112**, 535–542.

Binsted, N. & Hasnain, S. S. (1996). *J. Synchrotron Rad.* **3**, 185–196.

Binsted, N., Strange, R. W. & Hasnain, S. S. (1992). *Biochemistry*, **31**, 12117–12125.

Blackburn, N. J., Hasnain, S. S., Pettingill, T. M. & Strange, R. W. (1991). *J. Biol. Chem.* **34**, 23120–23127.

Blackburn, N. J., Strange, R. W., McFadden, L. M. & Hasnain, S. S. (1987). *J. Am. Chem. Soc.* **109**, 7162–7170.

Cheung, K. C. (1998). PhD thesis. *Development of XAFS for Multi-Dimensional Structural Information.* De Montfort University, Leicester, England.

Cramer, S. P., Tench, O., Yocum, M. & George, G. N. (1988). *Nucl. Instrum. Methods A*, **266**, 586–591.

Cunane, L. M., Chen, Z. W., Durley, R. C. E. & Mathews, F. S. (1996). *Acta Cryst.* D**52**, 676–686.

Dauter, Z., Lamzin, V. S. & Wilson, K. S. (1997). *Curr. Opin. Struct. Biol.* **7**, 681–688.

Derbyshire, G., Cheung, K. C., Sangsingkeow, P. & Hasnain, S. S. (1999). *J. Synchrotron Rad.* **6**, 62–62.
Dodd, F. E., Abraham, Z. H. L., Eady, R. R. & Hasnain, S. S. (2000). *Acta Cryst.* D**56**, 690–696.
Dodd, F. E., Hasnain, S. S., Hunter, W. N., Abraham, Z. H. L., Debenham, M., Kanzler, H., Eldrige, M., Eady, R. R., Ambler, R. P. & Smith, B. E. (1995). *Biochemistry*, **34**, 10180–10186.
Durley, R., Chen, L., Lim, L. W., Scott Mathews, F. & Davidson, V. L. (1993). *Protein Sci.* **2**, 739–752.
Ellis, P. J. & Freeman, H. C. (1995). *J. Synchrotron Rad.* **2**, 190–195.
Engh, R. A. & Huber, R. (1991). *Acta Cryst.* A**47**, 392–400.
Frahm, R. (1989). *Rev. Sci. Instrum.* **60**, 2515–2518.
Groenveld, C. M., Feiters, M. C., Hasnain, S. S., Van Rijn, J., Reedijk, J. & Canters, G. W. (1986). *Biochim. Biophys. Acta*, **873**, 214–227.
Gurman, S. J., Binsted, N. & Ross, I. (1984). *J. Phys. C*, **17**, 143–151.
Gurman, S. J., Binsted, N. & Ross, I. (1986). *J. Phys. C*, **19**, 1845–1861.
Guss, J. M., Bartunik, H. D. & Freeman, H. C. (1992). *Acta Cryst.* B**48**, 790–811.
Guss, J. M., Harrowell, P. R., Murata, M., Norris, V. A. & Freeman, H. C. (1986). *J. Mol. Biol.* **192**, 361–387.
Hasnain, S. S. & Hodgson, K. O. (1999). *J. Synchrotron Rad.* **6**, 852–864.
Hedin, L. & Lundqvist, S. (1969). *Solid State Phys.* **23**, 1.
King, H. E. & Prewitt, C. T. (1979). *Am. Mineral.* **64**, 1265.
Konnert, J. H. & Hendrickson, W. A. (1980). *Acta Cryst.* A**36**, 344–350.
Lommen, A., Pandya, K. I., Koningsberger, D. C. & Canters, G. W. (1991). *Biochim. Biophys. Acta*, **1076**, 439–447.
McFadden, D. L., McPhail, A. T., Garner, C. D. & Mabbs, F. F. (1975). *J. Chem. Soc. Dalton Trans.*, pp. 263.
Morrell, C., Bilsborrow, R. L. & Derbyshire, G. E. (1989). Daresbury Laboratory Technical Memorandum DL/Sci/TM63E, pp. 1–12. Warrington: Daresbury Laboratory.
Murphy, L. M., Dobson, B. R., Neu, M., Ramsdale, C. A., Strange, R. W. & Hasnain, S. S. (1995). *J. Synchrotron Rad.* **2**, 64–69.
Murphy, L. M., Hasnain, S. S., Strange, R. W., Harvey, I. & Ingledew, W. J. (1991). *X-ray Absorption Fine Structure*, edited by S. S. Hasnain, pp. 152–155. Chichester: Ellis–Horwood.
Murphy, L. M., Strange, R. W. & Hasnain, S. S. (1997). *Structure*, **5**, 371–379.
Mustre de Leon, J., Rehr, J. J., Zabinsky, S. I. & Albers, C. (1991). *Phys. Rev. B*, **44**, 4146–4156.
Natoli, C. R., Benfatto, M. & Doniach, S. (1986). *Phys. Rev. A*, **34**, 4682.
Penner-Hahn, J. E., Murata, M., Hodgson, K. O. & Freeman, H. C. (1989). *Inorg. Chem.* **28**, 1826–1832.
Rehr, J. J., de Leon, J. M., Zabinsky, S. I. & Albers, R. C. (1991). *J. Am. Chem. Soc.* **113**, 5135–5140.
Romero, A., Nar, H., Huber, R., Messerschmidt, A., Kalverda, A., Canters, G. W., Durley, R. & Scott Mathews, F. (1994). *J. Mol. Biol.* **236**, 1196–1211.
Scott, R. A., Hahn, J. E., Doniach, S., Freeman, H. C. & Hodson, K. O. (1982). *J. Am. Chem. Soc.* **104**, 5364–5369.
Shepard, W. E. B., Anderson, B. F., Lewandoski, D. A., Norris, G. E. & Baker, E. N. (1990). *J. Am. Chem. Soc.* **112**, 7817–7819.
Stern, E. A., Ma, Y. J., Hanskepetitpierre, O. & Bouldin, C. E. (1992). *Phys. Rev. B*, **46**, 687–694.
Strange, R. W., Blackburn, N. J., Knowles, P. F. & Hasnain, S. S. (1987). *J. Am. Chem. Soc.* **109**, 7157–7162.
Strange, R. W., Dodd, F. E., Abraham, Z. H. L., Grössmann, J. G., Brüser, T., Eady, R. R., Smith, B. E. & Hasnain, S. S. (1995). *Nature Struct. Biol.* **2**, 287–292.
Strange, R. W., Murphy, L. M., Karlsson, B. G., Reinhammar, B. & Hasnain, S. S. (1996). *Biochemistry*, **35**, 16391–16398.
Strange, R. W., Reinhammar, B., Murphy, L. M. & Hasnain, S. S. (1995). *Biochemistry*, **34**, 220–231.